Composites Science and Technology 72 (2012) 1012–1019

Contents lists available at SciVerse ScienceDirect

Composites Science and Technology

journal homepage: www.elsevier.com/locate/compscitech

Bio-inspired tapered fibers for composites with superior toughness

Heide Humburg, Deju Zhu, Samia Beznia, Francois Barthelat *

Department of Mechanical Engineering, 817 Sherbrooke Street West, McGill University, QC, Canada H3A 2K6

ARTICLE INFO

Article history:
Received 15 November 2011
Received in revised form 6 February 2012
Accepted 13 March 2012
Available online 21 March 2012

Keywords:
A. Short-fiber composites
B. Fracture toughness
C. Fiber bridging
C. Modelling
Biomimetics

ABSTRACT

The toughness of fiber-reinforced composites largely relies on crack bridging. More specifically, intact fibers left behind the tip of a propagating crack are progressively pulled out of the matrix, dissipating energy which translates into toughness. While short fibers are traditionally straight, recent work has showed that they can be shaped to increase the pullout strength, but not necessarily the energy to pullout. In this work we have modeled, fabricated and tested short fibers with tapered ends inspired from a high-performance natural material: nacre from mollusc shells. The main idea was to duplicate a key mechanism where a slight waviness of the inclusion can generate strain hardening and energy dissipation when the inclusion is pulled out. We have incorporated a similar feature to short fibers, in the form of tapered ends with well defined opening angles. We performed pullout tests on tapered steel fibers in epoxy matrices, which showed that the pullout of tapered fiber dissipates up to 27 times more energy than straight fibers. The experimental results also indicated the existence of an optimum taper angle to maximize work of pullout while preventing the brittle fracture of the matrix. An analytical model was developed to capture the pullout mechanism and the interaction between fiber and matrix. The analytical model can guide the design of tapered fibers by providing predictions on the influence of different parameters.

1. Introduction

Stiffness, toughness and strength are highly desirable properties for structural materials. In short-fiber reinforced composites (SFRCs), these properties are largely controlled by the interfaces between the fibers and the matrix. These interfaces must be strong enough to transfer stresses between the matrix and the fibers to promote high modulus and strength, yet weak enough to allow for fiber debonding and fiber pullout, which are critical for toughness [1,2]. The toughness of well-designed short-fiber composites is mainly produced by fiber pullout. In the ideal scenario, when the material endures extreme stresses a crack may propagate in the matrix and will intersect some fibers which remain intact behind the crack front, exerting a closure force on the crack. As the crack faces spread apart these fibers debond from the matrix, and energy is dissipated through frictional sliding of the fiber on the matrix [3]. The amount of frictional force is a function of the friction coefficient and of the normal force at the matrix–fiber interface, which is provided by residual compression in the matrix from the curing and cooling process. Successful toughening is therefore conditional on these mechanisms, which will only occur with proper design of the material (alignment and density of the fibers, aspect ratio of the fibers, interfacial strength, and residual stresses) [4,5]. Ultimately the improvement in toughness is controlled by the energy dissipated in the pullout process, which is typically measured from a single fiber pullout test [6,7].

Careful design of the fiber–matrix interface is therefore critical and it can be achieved, for example, by fiber sizing or chemical functionalization [8,9]. Another approach to tailoring the pullout response of individual fibers is fiber shaping. Residual compressive stresses in the matrix impose a normal pressure on the interface, which generate frictional forces that are partially controlled by the surface roughness of the fibers [10]. Another approach is to alter the macroscopic shape of the fiber by introducing enlarged ends [1,11,12], flat and ripple ends [13,14] which effectively anchor the fibers in the matrix and enhance their overall mechanical performance. Fracture mechanics applied to composite materials demonstrates that the energy to pullout of individual fibers has a direct impact on the overall toughness of a composite made of such fiber. This principle has been demonstrated experimentally in the past, including for shaped fibers. For example, Zhu et al. [15] studied polyethylene fiber/polyester matrix systems and found that composites with shaped fibers were 9 times stronger and 17 times tougher than composites with straight fibers. Likewise, Bagwell and Wetherhold [16] conducted four-point bending tests on an end-shaped copper fiber/epoxy matrix composites and found an improvement in fracture toughness of 49% compared to straight fiber composites. These two studies demonstrated how shaped fibers, by altering the transfer of load between fiber and matrix,

* Corresponding author.
E-mail address: francois.barthelat@mcgill.ca (F. Barthelat).

0266-3538/$ - see front matter
http://dx.doi.org/10.1016/j.compscitech.2012.03.013

can significantly improve the overall strength and toughness of composites. The most interesting feature is the observed pullout-hardening, which is defined as the slope of the load–displacement curve after debonding. The steeper the slope the more the fiber resists pullout at a crack plane and therefore exhibits crack-bridging and crack-closure forces that reduce the stress intensity factor at the crack tip [17]. The displacement over which the hardening occurs is also of great importance, as it determines the pullout-distance that the fiber can travel without complete pullout leading to failure of the material. However, a too large end-shape can have deteriorative effects, since the fiber ends have a tendency to initiate matrix cracks [15]. If properly designed, intact tapered fibers can transfer sufficient load after first cracking to allow the composite to undergo multiple cracking and spread debonding and pullout over larger volumes [18]. This would allow a significant amount of deformation before a crack localizes and the composite fails. In these systems the geometry of the fiber was significantly altered, which firmly anchored the fiber to the matrix and increased the pullout force. However, the locking between fiber and matrix is so strong that sliding and energy dissipation was limited. Interestingly, a similar design problem was solved in nature in mollusk shells, a five million year old natural composite material. In particular, nacre (mother of pearl) is made of microscopic mineral tablets which provide stiffness and hardness. Under tensile stress the tablets can slide and pullout from one another, dissipating a tremendous amount of energy which translates into toughness: Nacre is 3000 times tougher than the mineral it is made of [19]. An important requirement for this behavior is hardening. As tablets slide a mechanism must make it slide further so that tablet sliding spreads over large volumes. The structural feature which generates strain hardening in nacre was recently identified as dovetail-like features at the ends of tablets (Fig. 1a) [20]. This feature generates progressive locking as the tablets are pulled out (Fig. 1b), which generates hardening, makes pullout stable and generates toughness at the macroscale [20].

The waviness of the tablets – a very simple geometrical feature – is therefore a key mechanism for the high toughness of nacre, leading to stable crack propagation and crack-arresting capabilities. This type of insights into the performance of natural materials can inspire similar designs in engineering materials, through a process called biomimetics [21]. For example, in recent work the waviness of the tablets has been successfully implemented into macro-composites which duplicated the remarkable behavior of nacre in tension [22,23]. In this work we applied the concepts of dovetail, progressive locking, hardening and energy dissipation to short fibers.

2. Tapered fiber geometry: overview and impact on toughness

Incorporating short fibers with tapered ends into a ductile matrix is expected to alter the deformation and fracture mechanisms significantly (Fig. 2). In the presence of a macroscale crack the tapered fibers bridging the crack will pull out of crack faces and "plow" through the ductile matrix, adding viscoplastic energy dissipation to frictional dissipation. In terms of force response the taper is expected to greatly increase the force and energy to pullout, which will result in enhanced toughness at the macroscale. In addition, the pullout force will rise progressively to its maximum value as the pullout distance increases, generating deformation hardening. As a result, fibers will start debonding in other sites in the neighborhood ahead of the main crack, generating secondary cracks. In the optimum case, we anticipate that the locking of the fiber can be strong enough to develop a "process zone" ahead of the main crack, consisting of micro-cracks that are stabilized by the tapered fibers. While such material is not available yet in engineering form, a natural material like nacre demonstrates that this mechanism is feasible.

3. Pullout experiments

As a first step to developing the material described above, we performed pullout tests on short stainless steel fibers with different tapered angles. Millimeter size stainless steel shaft and hollow truncated cones with five different opening angles (0°, 2°, 5°, 10° and 20°) were machined. The ends of the shafts and the inner cavity of the cones were threaded so the cones were mounted at the ends of the shafts to form the required tapered fibers. This two-step fabrication process was found to be the most efficient and accurate approach to machine small fibers with high aspect ratio, with dimensions showed in Fig. 3a. The fibers were cleaned with acetone prior to embedding in the matrix.

The matrix was prepared from a two component room-temperature cure epoxy (Miapoxy 100/95, MIA Chemicals Inc., Avon, Ohio, USA) mixed in a weight ratio 100:24 and stirred thoroughly until the resin appeared clear and transparent. The mixture was subjected to vacuum at room temperature for 10 min for degassing, and was immediately poured into cylindrical molds with a diameter of 26 mm. The fiber was then partially embedded in the matrix over a length of about 8 mm, and positioned with a custom-made holder to ensure that the axis of the fiber was aligned with the axis of the cylindrical matrix. The system was cured at 24 °C ± 2 °C for 24 h, followed by applying a post cure at 65 °C ± 2 °C for 6 h to achieve full cure. The resulting samples consisted of an epoxy cylinder with a partially embedded fiber emerging perpendicularly to the top surface. The embedded length was measured on each sample and was found to be 8.3 mm ± 0.2 mm. The sample was then extracted from the mold and mounted in a universal testing machine (MTS Insight, 5 kN load cell, MTS Systems Corp., USA). The epoxy cylinder was held with a custom-made aluminum fixture, while the lower end of the fiber was mounted in a coupling nut and in the jaws of the loading machine (Fig. 3b). The upper cross-head was moved at a constant speed of 1 mm/min, while pullout

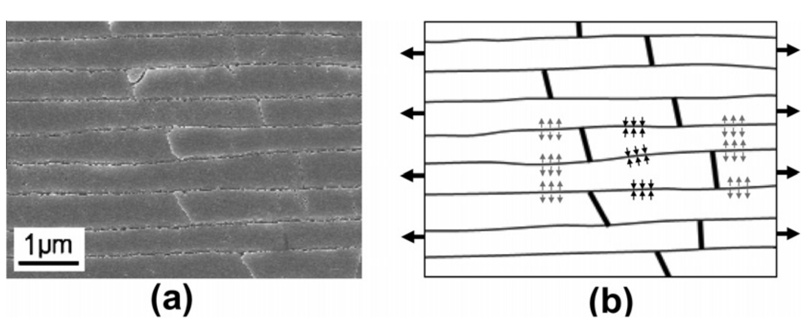

Fig. 1. (a) SEM-picture of nacre revealing the waviness of the aragonite tablets. Under tensile load (b) this geometry creates compressive stresses that prevent further sliding of the platelets and delay crack-localization.

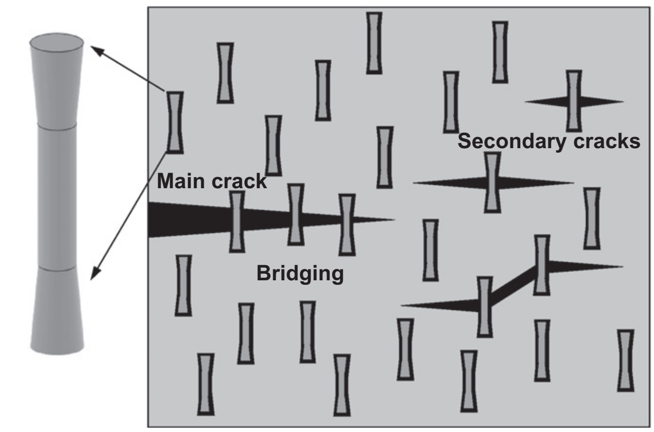

Fig. 2. Schematic depiction of the crack-bridging capacities of tapered fibers exhibiting a closure force on the crack through interlocking with the matrix. Although the schematic shows aligned fibers, similar mechanisms can be expected for fibers with random orientation.

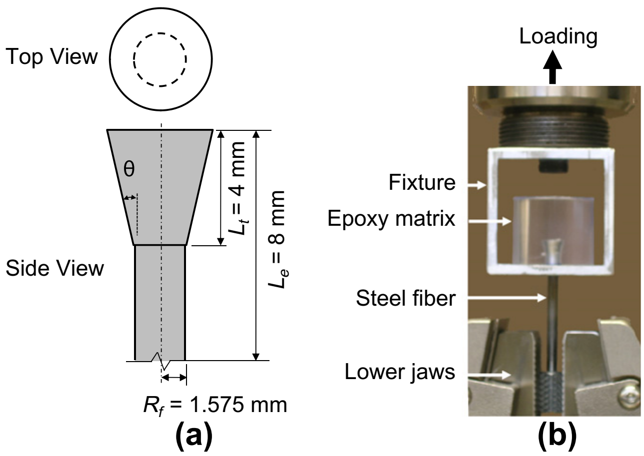

Fig. 3. (a) Dimensions of the tapered fiber; and (b) single fiber pullout testing setup.

force and displacement were recorded by a digital data acquisition system (MTS TestWorks® Software). In addition, a digital camera mounted on a tripod was used to capture pictures of the sample during the experiment. In order to assess the effect of friction between tapered fiber and epoxy matrix on the pullout behavior, another set of fibers was coated with a release agent (Chemlease® 15 Sealer/70-90 Release Agent, Chem-Trend L.P., Howell, USA) prior to embedding in order to reduce the friction between fiber and matrix [24,25]. The resulting pullout force–displacements curves for treated and untreated fibers are shown in Fig. 4a and b.

As expected, the maximum pullout force increased significantly with taper angle. The interfaces of straight fibers ($\theta = 0°$) failed at a pullout force of 600 N (untreated) and 100 N (treated), which was followed by a continuous decrease of the pullout force until complete pullout (at a displacement equal to the embedded length, about 8 mm). In the $\theta = 0°$ cases the frictional force which provides resistance, is generated by the normal pressure on the interface from residual compression in the matrix due to shrinkage during the curing stage. The normal pressure on the interface being constant and the contact area between fiber and matrix decreasing linearly with pullout distance, the pullout force also decreased linearly (Fig. 4). Pullout forces were lower with treated fibers since the interface coefficient of friction was lower. While the initial stiffness and the debonding force of tapered fibers were similar to those of the straight fibers, the introduction of the tapers altered the shape of the curve dramatically (Fig. 4). The force kept increasing with pullout distance even after debonding. Driving the tapered fiber "plowed" the deformable matrix and enlarged the initial cavity in the matrix, as seen on some of the snapshots of Fig. 5. The stresses required to deform the matrix translated into an additional normal force on the interface, and therefore to additional frictional resistance and pullout force. This powerful mechanism generated the hardening associated with pullout, as well as the high maximum pullout force. Meanwhile, the contact area between fiber and matrix decreased as the fiber was pulled out, so that at a pullout distance of about 2.5 mm the pullout force reached its maximum value and decreased, until complete pullout. This progressive locking effect and maximum pullout force was magnified with greater taper angle and higher friction coefficient (Fig. 4). However, instances of premature matrix failure occurred as taper angle was increased. Fig. 5a shows pictures taken during the pullout of a 5° taper angle fiber, where a penny crack appeared and progressively grew to eventually fracture the matrix entirely. Fig. 5b shows another example of a 10° taper angle fiber where the matrix catastrophically failed after a short pullout distance. These cases of matrix failure are detrimental because all the beneficial mechanisms of energy dissipation are terminated prematurely. For those cases matrix failure interrupted the pullout force–displacement curves (Fig. 4a and b). The ends of short fibers generate stress concentrations in the matrix, which weaken the system even for the case of straight fibers. Tapered fibers, because of their geometry, may increase the severity of these stress concentration. Hasebe and Iida [26] established relations between the stress intensity factor of the corner with an arbitrary angle and the stress concentration factor. According to their results, the increase of stress concentration factor is less than 10% when the corner angle decreases by 20°. The tapered fibers tested in this work therefore did not significantly increase stress concentrations in the matrix.

In one 20° sample with untreated fibers the pullout was not completed because the loading machine reached its maximum load capacity (this data was excluded from further analysis). Fig. 4a and b were used to compute the maximum pullout force (F_{max}) as well as the work of pullout (WOP), which is the area under the force–displacement curves up to the point where either the fiber pulls out or the matrix fails. Fig. 6a shows how the maximum pullout force continuously increased with taper angle. One the other hand, Fig. 6a shows a different trend for the WOP. The WOP increased with taper angle up to a maximum of about 10 J for a 5° taper angle, as a result of enhanced energy dissipation in the matrix. However, the WOP decreases thereafter because of premature matrix failure. For this set of materials and overall fiber dimension an angle of 5° is therefore the optimum angle for energy dissipation, which is 10–27 times higher than the energy dissipated by a straight fiber of similar dimensions (depending on whether the fiber was treated or not). As emphasized in the introduction this type of improvement in pullout energy is expected to directly translate into enhanced toughness.

Our results also confirm that friction coefficient has a significant effect on F_{max} and WOP. For all tested angles, the results of the untreated fibers were higher than those of their treated counterparts, indicating a higher interfacial bonding strength and coefficient of friction. The application of a release agent resulted in a WOP reduction of 65% for straight fiber, but only resulted in a reduction of 14–20% for tapered fibers. This indicates that the WOP of tapered fibers is less sensitive to coefficient of friction. Likewise, the pullout energy for the 5° case is about 10 times the energy dissipated for a straight fiber when both straight and tapered fibers are untreated. For the case of treated fibers with lower friction coefficient, 5° tapered fibers dissipated on average 27 times the energy

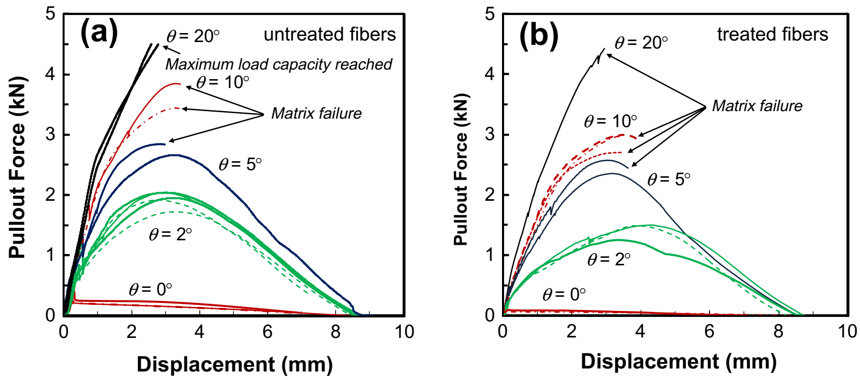

Fig. 4. Experimental pullout curves of (a) untreated fibers, and (b) treated fibers with release agent.

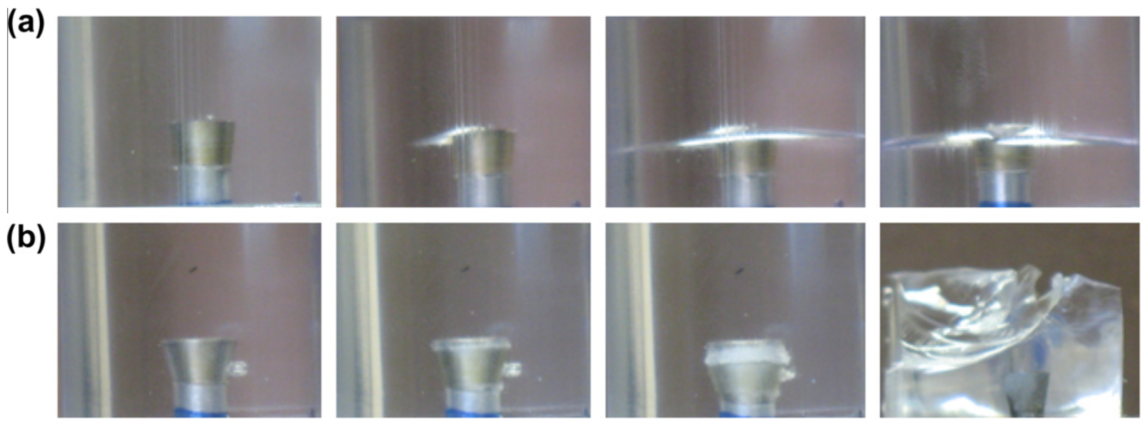

Fig. 5. (a) Pullout process of a 5° taper angle fiber. Initial cracks developed at the embedded fiber tip, propagated and formed a complete cross-sectional crack before failure. (b) Pullout process of a 10° taper angle fiber with catastrophic matrix failure.

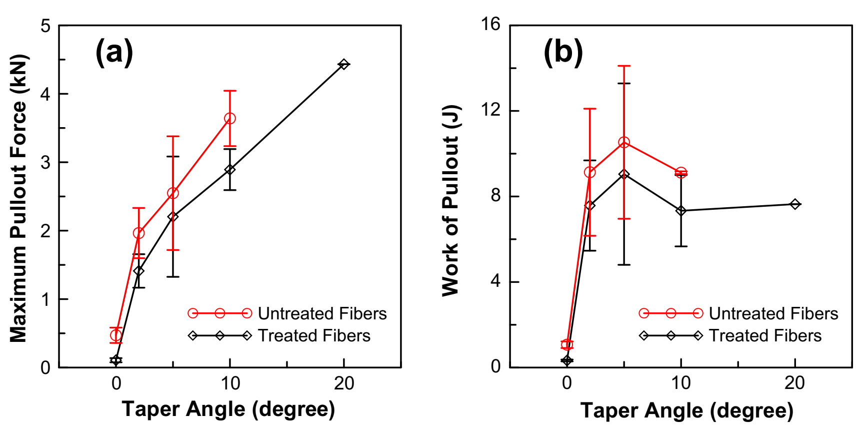

Fig. 6. (a) Maximum pullout force and (b) work of pullout (WOP) versus taper angle for untreated and treated fibers. The data points show the average values and the bars show the range for each tested angle.

dissipated in the pullout of a straight fiber. The benefits of tapering fibers are therefore more pronounced for interfaces with low coefficient of friction. While the frictional resistance is the most important factor contributing to WOP for straight fibers [11], elastic and plastic deformation of the matrix due to fiber–matrix interference gain more importance during the pullout of tapered fibers. These findings are confirmed by experimental results from Wetherhold and Lee [12], who found that the advantage of end-shaped fibers over unmodified fibers to be higher for weaker interfaces.

4. Analytical model

In order to better understand the mechanics and critical parameters involved in the pullout of a tapered fiber we have developed a simplified analytical model. The model relies on the simplifying assumptions that (i) the interaction fiber–matrix is dominated by the interference between fiber and matrix, (ii) the fiber is rigid compared to the matrix, and (iii) this interference problem can be treated as the "sum" of two-dimensional plane strain problems with the out-of-plane axis coinciding with the axis of the fiber, following [27,28]. Fig. 7a shows the end of a tapered fiber, modeled here as a rigid truncated cone of root radius R_0, length L_t and taper angle θ. In the steady state regime of fiber pullout, the cone plows through the matrix along a pre-existing cavity of radius R_0, which would contain the central shaft of the fiber in the actual system. In this process, the rigid cone "forces" the matrix cavity to enlarge its radius by a distance δ called interference (Fig. 7b), which is a function of the taper angle and position z along the cone axis. The deformation imposed on the matrix by the interference results in a distribution of interfacial pressures P_i, which will in turn generate (i) additional resistance along the direction of the fiber and (ii) additional frictional forces. These two effects combined give raise to the pullout force F (Fig. 7b). Given the large interference distances developed in this process the matrix is likely to undergo plastic deformations, which was also considered in the model (Fig. 7b). After plowing, the taper leaves a cavity in the matrix, of radius equal to the maximum radius of the taper.

The interference, elastic–plastic deformation of the matrix, interface pressure and stress transfer to the tapered fiber end were all captured in a simplified model detailed in Appendix. The main result from this model is the average axial stress in a section of the fiber as function of position z:

$$\bar{\sigma}_{zz}(z) = -\int_0^{L_t} \frac{2}{R_0 + z\tan\theta} P_i(f + \tan\theta)dz \tag{1}$$

where f is the coefficient of friction, and R_0, L_t and θ are the dimensions of the taper (Fig. 7a). P_i, the pressure at the interface fiber–matrix, takes a different form depending on whether the matrix is elastic or elastic–plastic at that section (see Appendix for details). Once the stress distribution is computed the pullout force is given by:

$$F = \pi R_0^2 \bar{\sigma}_{zz}(z = 0) \tag{2}$$

The shrinkage of the matrix can be incorporated by adding an interference $R_0\varepsilon_S$ to the model, where ε_S is the shrinkage strain. This simple model captures the salient mechanisms of a tapered fiber pulling out of a deformable matrix, and can be used to assess the effect of key parameters for the fiber–matrix system. Fig. 8 shows the effect of the friction f, strength to stiffness ratio σ_y/E^* and shrinkage strain ε_S on the normalized steady state pullout force, which was taken as the pullout force divided by the pullout force for a straight fiber. Fig. 8 therefore provides a snapshot of how the taper "amplifies" pullout forces for various sets of parameters.

The reference values chosen to plot these results are close to the actual value of the system: f was evaluated at about 0.2, σ_y/E^* is about 0.02 and the shrinkage strain of epoxy matrix used in the experiments is about -0.01 (obtained by shrinkage test using a modified rheology method [29]). In all cases, Fig. 8 shows how the pullout force significantly increases as the taper angle is increased. Fig. 8a shows that the force amplification gained by tapered ends is the most dramatic for lower coefficient of friction, which confirms our experimental observations. This can be explained by Eq. (1), where the term $\tan\theta$ has more effect for lower values of f. Likewise, Fig. 8b shows that the force amplification is more pronounced for harder materials (higher σ_y/E^*). In the actual system the matrix undergoes plastic deformations, and therefore stronger matrix will provide more resistance to deformation and to plowing by the tapered fiber. Finally Fig. 8c shows that the force amplification is more pronounced when the curing shrinkage strain is smaller (in absolute value). Shrinkage generates an initial "pre-stress" on the interface fiber–matrix whose effects are added to those of plowing. In terms of energy, the model would generate the same trends as for maximum forces, since the pullout energy can be roughly estimated as $\frac{1}{2}L_tF_{\max}$. While our simplified model could not match the experimental values because of our simplifying assumptions, the trends it predicts are consistent with experiments, and the model can therefore be valuable for the future design of tapered fibers.

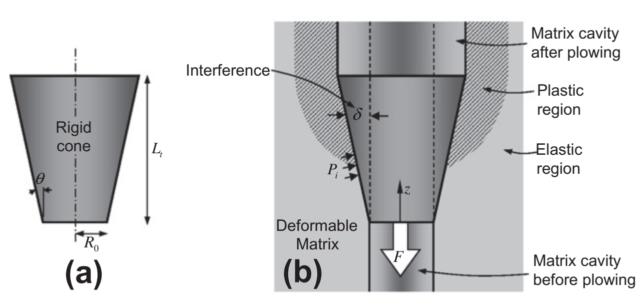

Fig. 7. Schematic diagrams of (a) the rigid truncated cone as a model for the tapered end of a fiber and (b) mechanics of plowing of this cone through an elastic–plastic matrix.

5. Summary and conclusions

The impact of bio-inspired tapers at the ends of fibers on maximum pullout force and energy dissipation was examined in this work. As in natural nacre which served as a "biomimetic" inspiration, the fibers generate highly stable pullout, with hardening leading to much higher maximum pullout force and energies dissipation than those of straight fibers of equivalent length and radius. An analytical model was developed, which also served as a tool for optimizing the tapered fiber shape in order to maximize the work of pullout. The current study provided the following results:

(1) The tapered fiber geometry was found to have a positive effect on $F_{\max}$ and WOP. It exceeds the results for straight fiber pullout 4–9 and 10–27 times respectively, and performs significant pullout-hardening.
(2) The experimental results indicate the existence of an optimum geometry to maximize WOP while preventing premature matrix failure.
(3) While it was not possible to directly compare our model with experiments because of the simplifying assumptions required to derive an analytical solution, the analytical model gives predictions which are consistent with the experiments, and which highlight the contribution of different parameters on the steady state pullout force. The tuning parameters are the taper angle θ, the tapered length L_t, the coefficient of friction f, and the mechanical properties (σ_y and E^*) of the matrix.

Even though the idea of a tapered fiber seems remote from natural nacre, the concepts in terms of structure and mechanisms are identical. In both nacre and fiber reinforced composites the fracture process is largely dominated by the pullout of stiff inclusions with high aspect ratio (fibers in fiber reinforced composites, mineral tablets in nacre). In both nacre and short fiber composites, the force required to initiate fiber pullout and the energy dissipated in the pullout process are controlled by mechanisms occurring at the interfaces between reinforcements and matrix. For example, the roughness of the reinforcement (fibers or tablets in nacre) has been shown, for both materials, to improve mechanical performance. Interestingly, the models developed by Evans and coworkers that capture the effect of asperities in nacre [30] were inspired by similar models developed 10 years earlier by the same author, for fiber composites [10]. In nacre, recent work [20] showed the importance of the profile of the tablets (waviness) to

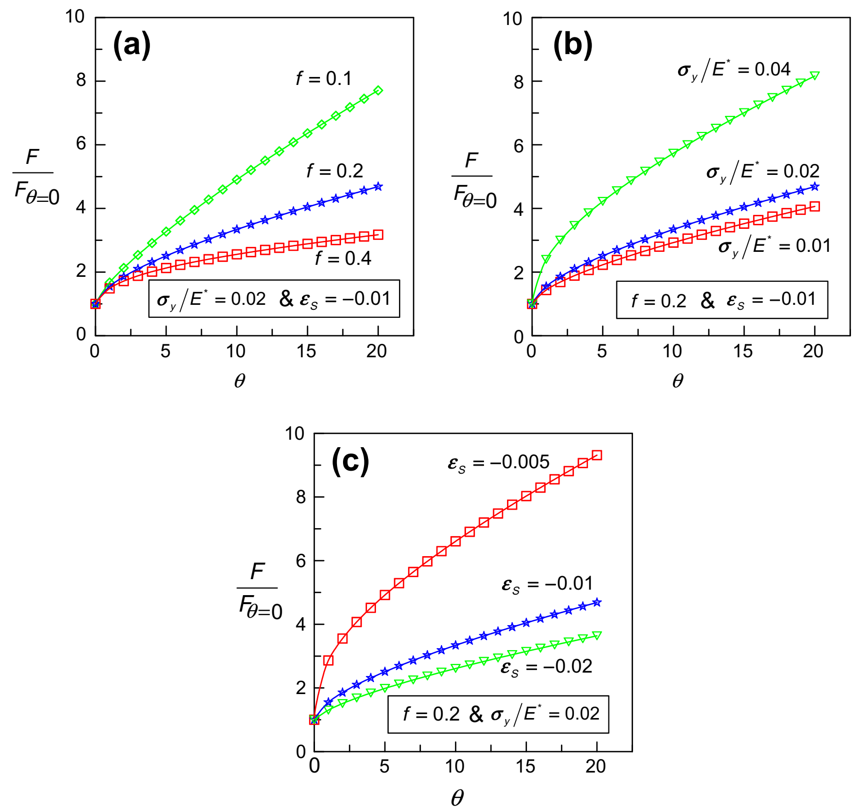

Fig. 8. Effect of the design parameters on the normalized steady state pullout force: (a) friction coefficient; (b) strength to stiffness ratio of epoxy matrix; (c) shrinkage strain.

generate progressive locking, hardening and energy dissipation. In this work we have "abstracted" this structure and mechanisms from natural nacre to implement it into fibers for reinforcements. Even though the structure may seem remote from natural nacre it is still a "bio-inspired" or "biomimetic" composite since it utilizes a key structure and mechanisms directly inspired from nacre.

The actual impact of the tapered geometry on overall toughness of the composite material is beyond the scope of this initial work and will be the topic of future research. Nevertheless, since energy to pullout has direct impact on toughness, multiplying the energy to pullout by a factor of 10 would lead to tremendous toughening effects. While it is difficult to predict how much toughness can be achieved until we actually fabricate a composite made of short tapered fibers, natural materials like nacre demonstrate the impressive performance that can be realized by well-defined and optimized microstructures and micromechanics.

Acknowledgements

This work was supported by the Faculty of Engineering at McGill University, by a Discovery Grant from the Natural Sciences and Engineering Research Council of Canada. Heide Humburg was supported by a scholarship from the Hans-Böckler-Foundation, Germany.

Appendix A

A.1. Interference

As the rigid, tapered fiber is pulled from the matrix it forces the matrix cavity to enlarge. More specifically, the radius of the cavity is increased by the so-called interference δ, which is a function of fiber pullout distance U and of position along the fiber z (Fig. 7b). In the steady state ($U > L_t$), the interference is $\delta = z \tan\theta$.

A.2. Elastic regime

The Lamé solution for an infinite, linear elastic matrix in plane strain can be used to predict the interface pressure P_i for a cavity or radius R subjected to an increase of radius δ:

$$P_i = E^* \frac{\delta}{R} \quad \text{where} \quad E^* = \frac{E}{1-\nu^2} \tag{A.1}$$

The radial and hoop stresses are then:

$$\sigma_{rr} = -\sigma_{\theta\theta} = -\left(\frac{R}{r}\right)^2 P_i \tag{A.2}$$

In particular, the highest stresses are at the interface $r = R$:

$$\sigma_{rr}(R) = -\sigma_{\theta\theta}(R) = -P_i = -E^* \frac{\delta}{R} \tag{A.3}$$

A.3. Condition for yielding

With sufficient stresses, yielding will start in the matrix near the interface with the fiber. Using the maximum shear stress criterion and assuming $\sigma_{rr} < 0$ and $\sigma_{\theta\theta} > 0$:

$$\tau_{\max} = \left|\frac{\sigma_{rr} - \sigma_{\theta\theta}}{2}\right| = \frac{\sigma_{\theta\theta} - \sigma_{rr}}{2} = \frac{\sigma_y}{2} \tag{A.4}$$

where σ_y is the yield strength of the matrix. Combining Eqs. (A.3) and (A.4), provides the interference required to initiate yielding:

$$\delta_y = \frac{1}{2} R \frac{\sigma_y}{E^*} \tag{A.5}$$

A.4. Elastic–plastic regime

To model this regime we assumed perfect plasticity. For $\delta > \delta_y$, the plastic region propagates around the fiber and over a region

$R < r < R_P$, while for $r > R_P$ the matrix remains elastic. In the elastic region ($r > R_P$) the stresses are given by:

$$\sigma_{rr}^{e} = -\sigma_{\theta\theta}^{e} = -P_{ep}\frac{R_P^2}{r^2} \tag{A.6}$$

where P_{ep} is the pressure at the interface between the plastic and elastic regions. The elastic stresses must satisfy the yielding condition at $r = R_P$, which gives:

$$P_{ep} = \frac{1}{2}\sigma_y \tag{A.7}$$

The displacements in the elastic region are then:

$$u^{e}(r) = \frac{1}{2}\frac{R_P^2}{r}\frac{\sigma_y}{E^*} \tag{A.8}$$

In the yielded region, stress equilibrium in polar coordinate and yield criterion (A.4) can be combined to produce:

$$\frac{\partial\sigma_{rr}}{\partial r} = \frac{\sigma_y}{r} \tag{A.9}$$

Integrate Eq. (A.9) and applying the boundary condition $\sigma_{rr}(r = R) = -P_i$ leads to:

$$\sigma_{rr}^{p} = \sigma_y \ln\left(\frac{r}{R}\right) - P_i \tag{A.10}$$

$$\sigma_{\theta\theta}^{p} = \sigma_y\left[1 + \ln\left(\frac{r}{R}\right)\right] - P_i \tag{A.11}$$

At the elastic–plastic interface $\sigma_{rr}^{e}(R_P) = \sigma_{rr}^{p}(R_P)$, combining Eqs. (A.6), (A.7), and (A.10) gives:

$$P_i = \sigma_y\left(\frac{1}{2} + \ln\left[\frac{R_P}{R}\right]\right) \tag{A.12}$$

The displacements in the plastic regime can now be calculated. Neglecting the elastic strains over the plastic strains incompressibility can be written:

$$\varepsilon_{rr} + \varepsilon_{\theta\theta} = 0 \quad \text{or} \quad \frac{\partial u_r}{\partial r} + \frac{u_r}{r} = 0 \tag{A.13}$$

The solution is

$$u^{p}(r) = \frac{R_P}{r}u_{ep} \tag{A.14}$$

where u_{ep} is radial displacement at elastic–plastic interface.

For continuity at the elastic–plastic interface $u^p(R_P) = u^e(R_P)$, which with Eq. (A.8) gives:

$$u^{p}(r) = \frac{1}{2}\frac{R_P^2}{r}\frac{\sigma_y}{E^*} \tag{A.15}$$

and in particular the interference at interface is

$$\delta = \frac{1}{2}\frac{R_P^2}{R}\frac{\sigma_y}{E^*} \tag{A.16}$$

Then transform Eq. (A.16) into

$$\frac{R_P}{R} = \sqrt{2\frac{\delta}{R}\frac{E^*}{\sigma_y}} \tag{A.17}$$

Substitute Eq. (A.17) into Eq. (A.12), the interference pressure in elastic–plastic regime is given by:

$$P_i = \frac{1}{2}\sigma_y\left(1 + \ln\left[2\frac{\delta}{R}\frac{E^*}{\sigma_y}\right]\right) \tag{A.18}$$

A.5. Solution of the steady state case

A force balance on a thin section of fiber of thickness dz provides the equilibrium equation:

$$\frac{\partial\bar{\sigma}_{zz}}{\partial z} = -\frac{2}{R}P_i(f + \tan\theta) \tag{A.19}$$

where $\bar{\sigma}_{zz}(z)$ is the average axial stress over a section of the fiber at a distance z from the root of the taper, and $R = R_0 + z\tan\theta$ is the fiber radius. Integrating Eq. (A.19) gives

$$\bar{\sigma}_{zz} = -\int_0^{L_t}\frac{2}{R_0 + z\tan\theta}P_i(f + \tan\theta)dz \tag{A.20}$$

In the elastic regime, the interference pressure is given by Eq. (A.1) and the interference is $\frac{\delta}{R} = \frac{1}{\frac{R_0}{z\tan\theta}+1}$, so the boundary between elastic and elastic–plastic regime is defined by:

$$z_e = \frac{R_0}{\left(2\frac{E^*}{\sigma_y} - 1\right)\tan\theta} \tag{A.21}$$

For $z < z_e$, the stress is

$$\bar{\sigma}_{zz}^{e} = -\int_0^{z_e}\frac{2}{R_0 + z\tan\theta}E^*\frac{z\tan\theta}{R}(f + \tan\theta)dz \tag{A.22}$$

In the elastic–plastic regime ($L_t > z > z_e$), the interference pressure is determined by Eq. (A.18), and the stress is

$$\bar{\sigma}_{zz}^{ep} = -\int_{z_e}^{L_t}\frac{1}{R_0 + z\tan\theta}\sigma_y\left(1 + \ln\left[2\frac{z\tan\theta}{R}\frac{E^*}{\sigma_y}\right]\right)(f + \tan\theta)dz \tag{A.23}$$

So the steady state pulling force is determined by multiplying the stress with the cross-section area of the fiber (πR_0^2),

$$F = \pi R_0^2\bar{\sigma}_{zz|z=0} \tag{A.24}$$

A.6. Curing shrinkage

The shrinkage of the matrix can be incorporated by simply adding an initial interference $R_0\varepsilon_S$ to the model, where ε_S is the absolute value of the shrinkage strain.

References

[1] Zhu YT, Valdez JA, Shi N, Lovato ML, Stout MG, Zhou SJ, et al. A composite reinforced with bone-shaped short fibers. Scripta Mater 1998;38(9):1321–5.
[2] Piggott M. The effect of aspect ratio on toughness in composites. J Mater Sci 1974;9(3):494–502.
[3] Mallick P. Fiber-reinforced composites: materials, manufacturing, and design. CRC Press; 2008.
[4] Zhu D, Peled A, Mobasher B. Dynamic tensile testing of fabric–cement composites. Constr Build Mater 2011;25(1):385–95.
[5] Li VC, Mishra DK, Wu HC. Matrix design for pseudo-strain-hardening fibre reinforced cementitious composites. Mater Struct 1995;28(10):586–95.
[6] Hampe A, Kalinka G, Meretz S, Schulz E. An advanced equipment for single-fibre pull-out test designed to monitor the fracture process. Composites 1995;26(1):40–6.
[7] Zhu D, Soranakom C, Mobasher B, Rajan SD. Experimental study and modeling of single yarn pull-out behavior of kevlar 49 fabric. Compos Part a-Appl S 2011;42(7):868–79.
[8] Yue CY, Padmanabhan K. Interfacial studies on surface modified Kevlar fibre epoxy matrix composites. Compos Part B-Eng 1999;30(2):205–17.
[9] George J, Sreekala M, Thomas S. A review on interface modification and characterization of natural fiber reinforced plastic composites. Polym Eng Sci 2001;41(9):1471–85.
[10] Evans AG, Zok FW, Davis J. The role of interfaces in fiber–reinforced brittle matrix composites. Compos Sci Technol 1991;42(1–3):3–24.
[11] Beyerlein IJ, Zhu YT, Mahesh S. On the influence of fiber shape in bone-shaped short-fiber composites. Compos Sci Technol 2001;61(10):1341–57.
[12] Wetherhold RC, Lee FK. Shaped ductile fibers to improve the toughness of epoxy–matrix composites. Compos Sci Technol 2001;61(4):517–30.
[13] Bagwell RM, Wetherhold RC. Improvement in fracture toughness of an epoxy/copper composite through the use of various end shaped fibers. Mat Sci Eng a-Struct 2003;361(1–2):294–301.
[14] Tsai JH, Patra A, Wetherhold R. Finite element simulation of shaped ductile fiber pullout using a mixed cohesive zone/friction interface model. Compos Part a-Appl S 2005;36(6):827–38.

[15] Zhu YT, Valdez JA, Beyerlein IJ, Zhou SJ, Liu C, Stout MG, et al. Mechanical properties of bone-shaped-short-fiber reinforced composites. Acta Mater 1999;47(6):1767–81.
[16] Bagwell RM, Wetherhold RC. End-shaped copper fibers in an epoxy matrix – predicted versus actual fracture toughening. Theor Appl Fract Mech 2005;43(2):181–8.
[17] Wetherhold RC, Bos J. Ductile reinforcements for enhancing fracture resistance in composite materials. Theor Appl Fract Mech 2000;33(2):83–91.
[18] Lin Z, Li VC. Crack bridging in fiber reinforced cementitious composites with slip-hardening interfaces. J Mech Phys Solids 1997;45(5):763–87.
[19] Barthelat F, Espinosa HD. An experimental investigation of deformation and fracture of nacre-mother of pearl. Exp Mech 2007;47(3):311–24.
[20] Barthelat F, Tang H, Zavattieri P, Li CM, Espinosa H. On the mechanics of mother-of-pearl: a key feature in the material hierarchical structure. J Mech Phys Solids 2007;55(2):306–37.
[21] Barthelat F. Biomimetics for next generation materials. Philos T R Soc A 2007;365(1861):2907–19.
[22] Barthelat F, Zhu D. A novel biomimetic material duplicating the structure and mechanics of natural nacre. J Mater Res 2011;26(10):1203–15.
[23] Espinosa HD, Rim JE, Barthelat F, Buehler MJ. Merger of structure and material in nacre and bone – perspectives on de novo biomimetic materials. Prog Mater Sci 2009;54(8):1059–100.
[24] Takaku A, Arridge R. The effect of interfacial radial and shear stress on fibre pull-out in composite materials. J Phys D Appl Phys 1973;6:2038.
[25] Zhu Y, Valdez J, Shi N, Lovato M, Stout M, Zhou S, et al. Influence of reinforcement morphology on the mechanical properties of short-fiber composites. In: Li B, editor. Processing of metals and advanced materials: modeling, design and properties, 1998. p. 251–60.
[26] Hasebe N, Iida J. Intensity of corner and stress-concentration factor. J Eng Mech-Asce 1983;109(1):346–56.
[27] Bozkaya D, Muftu S. Mechanics of the tapered interference fit in dental implants. J Biomech 2003;36(11):1649–58.
[28] Kerans RJ, Parthasarathy TA. Theoretical-analysis of the fiber pullout and pushout tests. J Am Ceram Soc 1991;74(7):1585–96.
[29] Khoun L, Hubert P. Cure shrinkage characterization of an epoxy resin system by two in situ measurement methods. Polym Compos 2010;31(9):1603–10.
[30] Evans AG, Suo Z, Wang RZ, Aksay IA, He MY, Hutchinson JW. Model for the robust mechanical behavior of nacre. J Mater Res 2001;16(9):2475–84.